SUPPLEMENTARY MATERIAL

Half-Sandwich Rhodium Complexes with Releasable N-Donor Monodentate Ligands: Solution Chemical Properties and Possibility for Acidosis Activation

János P. Mészáros [1,2,*], Wolfgang Kandioller [3,4], Gabriella Spengler [1,5],

Alexander Prado-Roller [3,4], Bernhard K. Keppler [3,4] and Éva A. Enyedy [1,2,*]

1 MTA-SZTE Lendület Functional Metal Complexes Research Group, University of Szeged, Dóm tér 7, H-6720 Szeged, Hungary
2 Department of Inorganic and Analytical Chemistry, Interdisciplinary Excellence Centre, University of Szeged, Dóm tér 7, H-6720 Szeged, Hungary
3 Institute of Inorganic Chemistry, Faculty of Chemistry, University of Vienna, Währinger Str. 42, A-1090 Vien-na, Austria
4 Research Cluster "Translational Cancer Therapy Research", University of Vienna, Währinger Str. 42, A-1090 Vienna, Austria
5 Department of Medical Microbiology, Albert Szent-Györgyi Health Center and Albert Szent-Györgyi Medical School, University of Szeged, Semmelweis utca 6, H-6725 Szeged, Hungary
* Correspondence: meszaros.janos@chem.u-szeged.hu (J.P.M.); enyedy@chem.u-szeged.hu (É.A.E.)

## CONTENTS

FIGURE S1.

Figure S1. UV-vis spectra of the [RhCp*(8HQH$_{-1}$)(H$_2$O)]$^+$ complex at different concentrations of econazole. Conditions are the same as in the stock solutions prepared for anticancer and antibacterial experiments (pH = 7.4 (phosphate buffer) with 50% (v/v) ethanol). {c([RhCp*(8HQH$_{-1}$)(H$_2$O)]$^+$) = 5 mM; c(econazole) = 0, 5 7.5 or 10 mM; t = 25 °C; ℓ = 0.2 cm}

# CHARACTERIZATION OF THE ISOLATED COMPLEXES: ¹H NMR AND ¹³C NMR SPECTROSCOPIC DATA
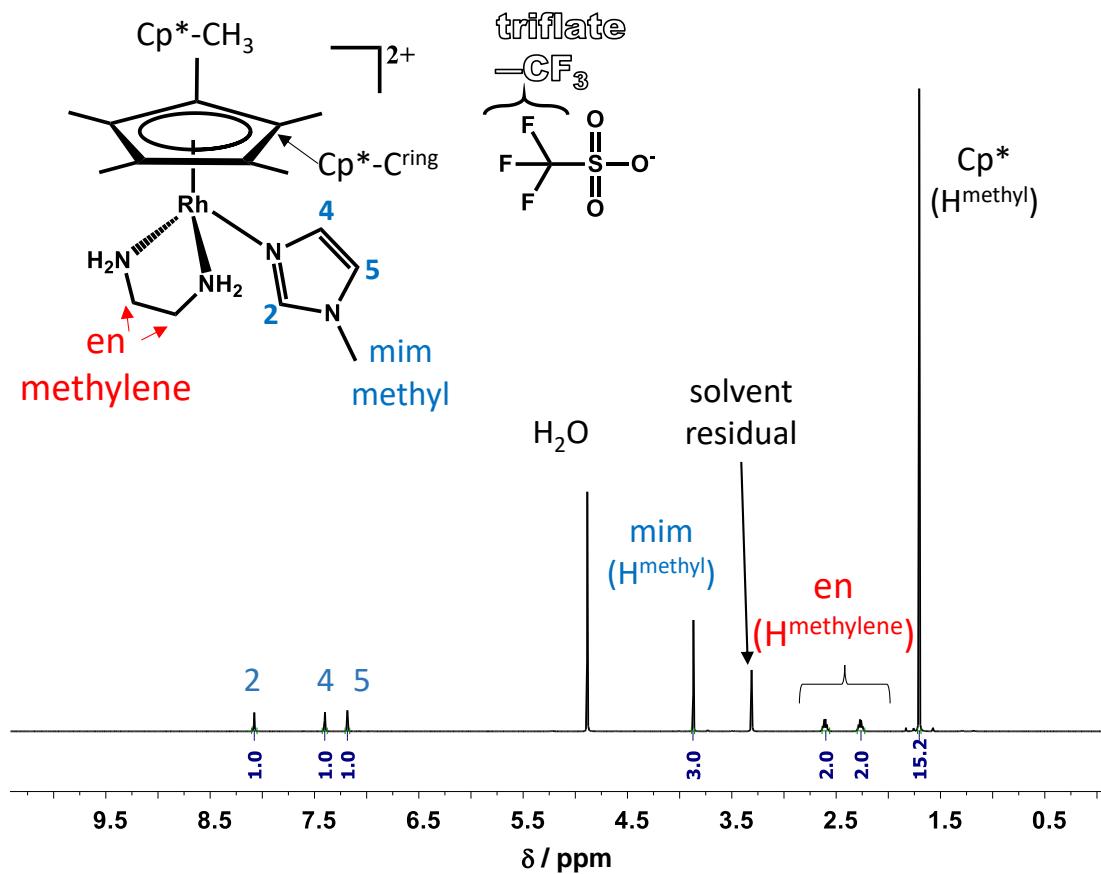
Figure S2. ¹H NMR spectrum of [RhCp*(en)(mim)](CF₃SO₃)₂ in CD₃OD. Inserted structure shows numbering of peaks. {c(complex) = 10 mM, t = 25.0°C}
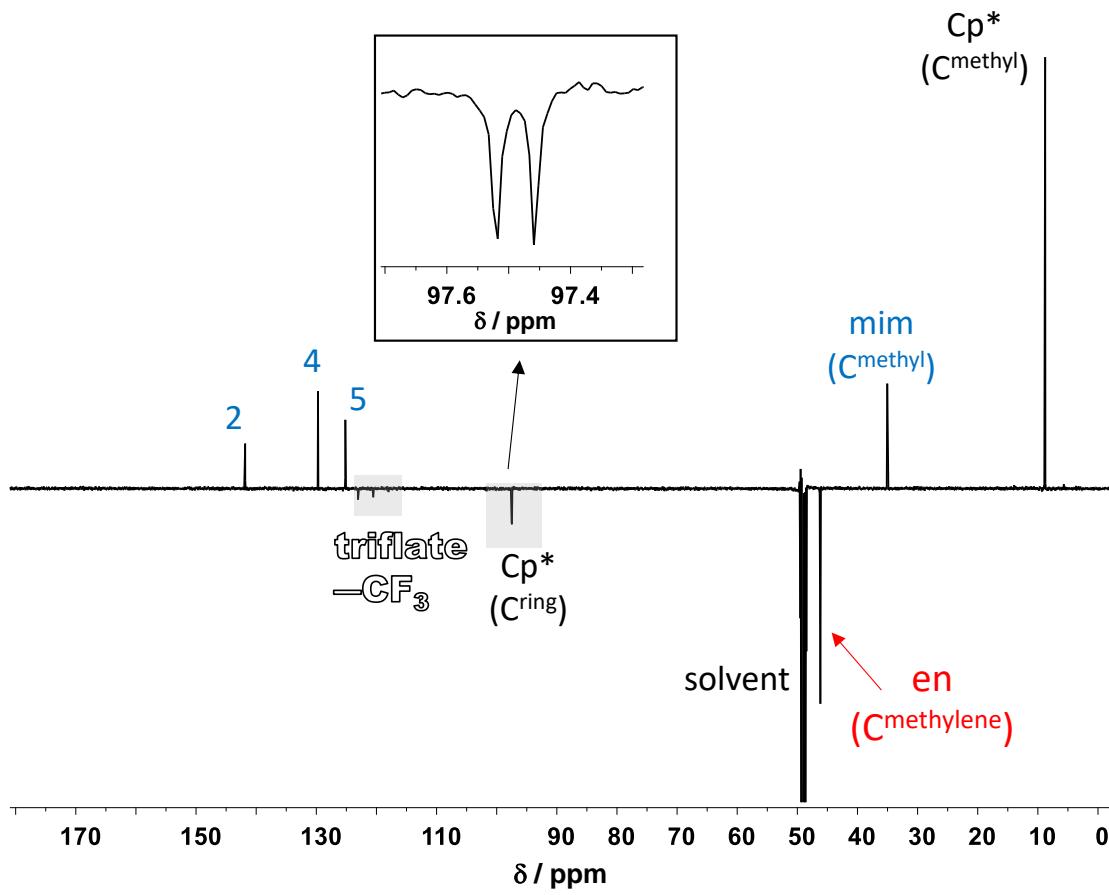
Figure S3. ^{13}C APT NMR spectrum of [RhCp*(en)(mim)](CF₃SO₃)₂ in CD₃OD. For numbering see **Figure S2**. Inserted figure shows the doublet of **Cp*** ring carbon atoms as a result of coupling with ^{103}Rh. {c(complex) = 10 mM, t = 25.0°C}
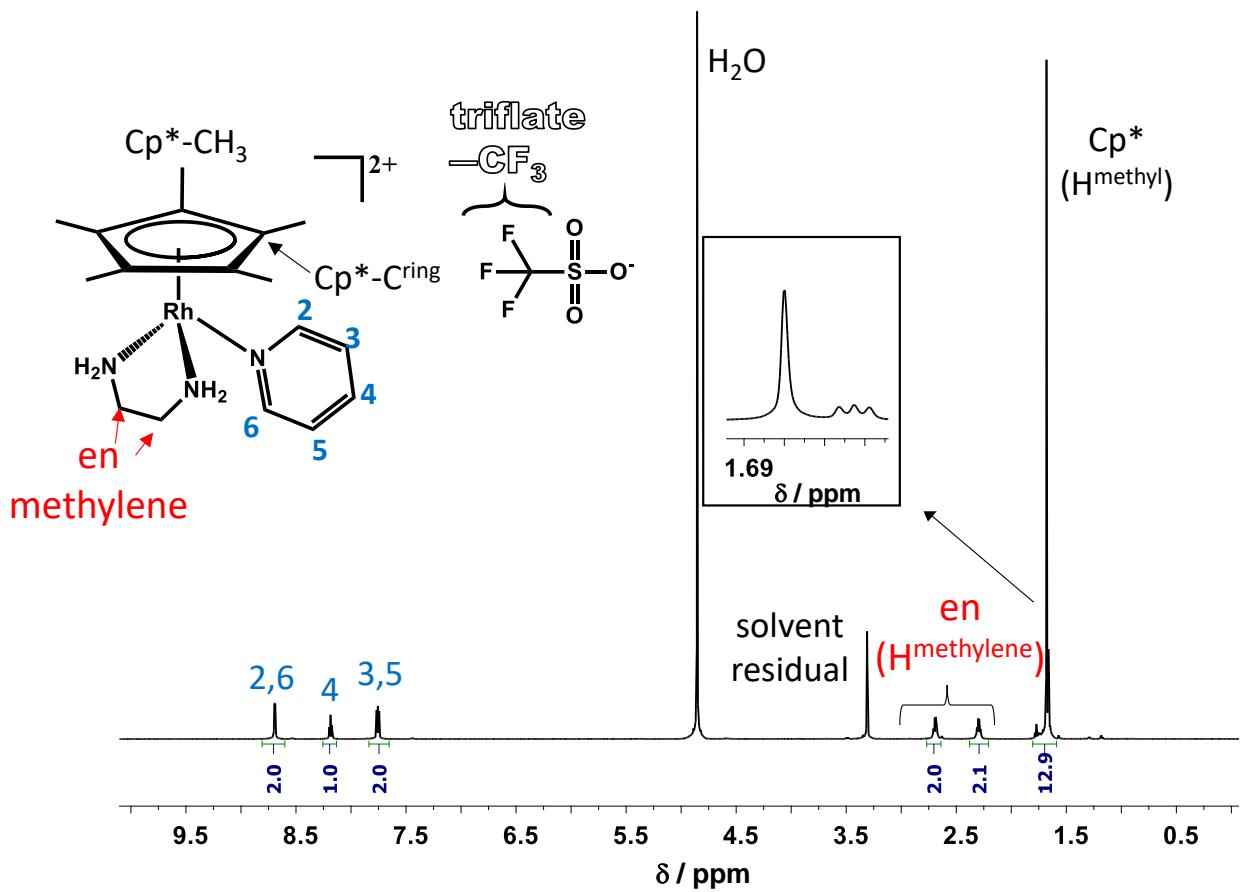
Figure S4. ^{1}H NMR spectrum of [RhCp*(en)(Py)](CF$_3$SO$_3$)$_2$ in CD$_3$OD. Inserted structure shows numbering of peaks. Inset shows a triplet indicating the presence of –CH$_2$D group. {c(complex) = 10 mM, t = 25.0°C}
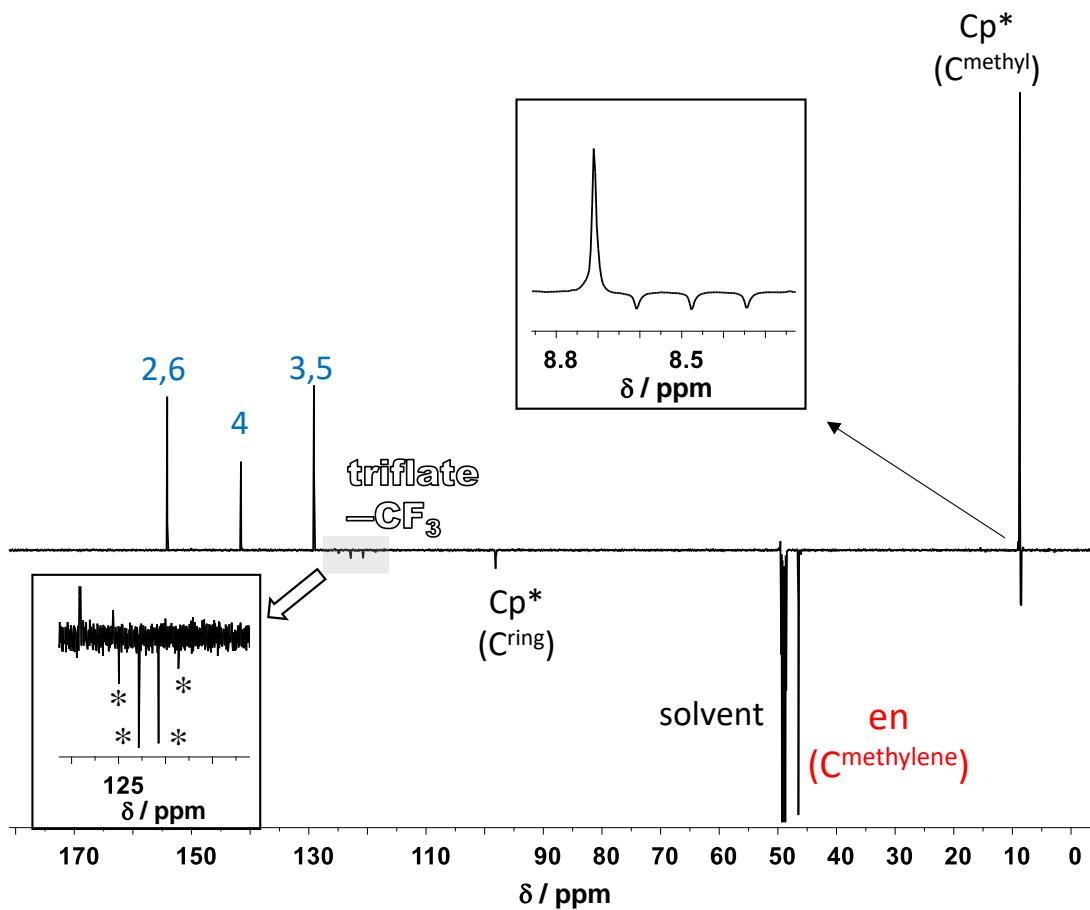
Figure S5. ^{13}C APT NMR spectrum of $[RhCp*(en)(Py)](CF_3SO_3)_2$ in CD_3OD. For numbering see **Figure S4**. Inserted figure shows the quartet of **–CF₃** carbon atom as a result of coupling with ^{19}F and a triplet indicating the presence of $–CH_2D$ group. {c(complex) = 10 mM, t = 25.0°C}
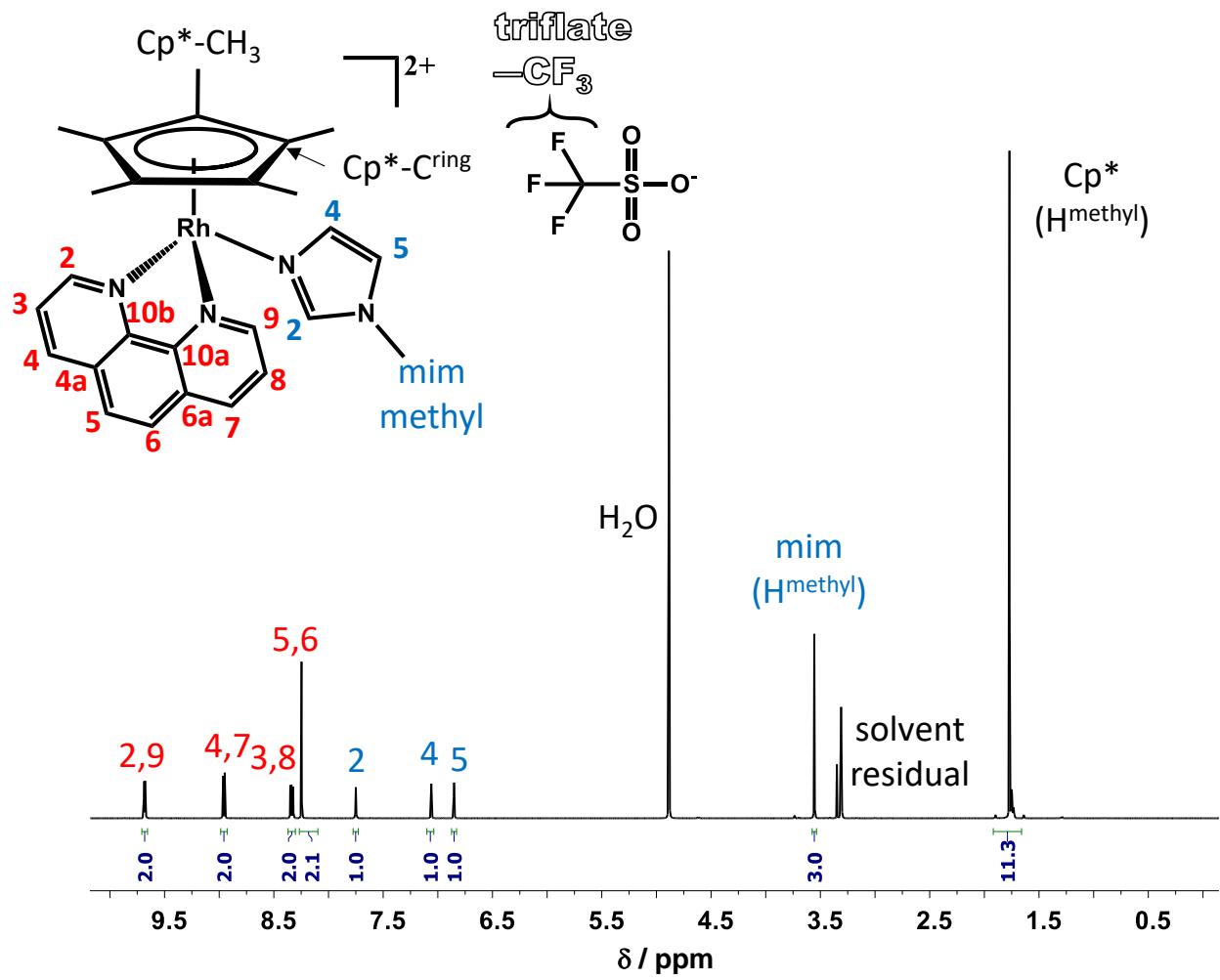
Figure S6. ^{1}H NMR spectrum of [RhCp*(phen)(mim)](CF3SO3)2 in CD3OD. Inserted structure shows the numbering of peaks. {c(complex) = 10 mM, t = 25.0°C}
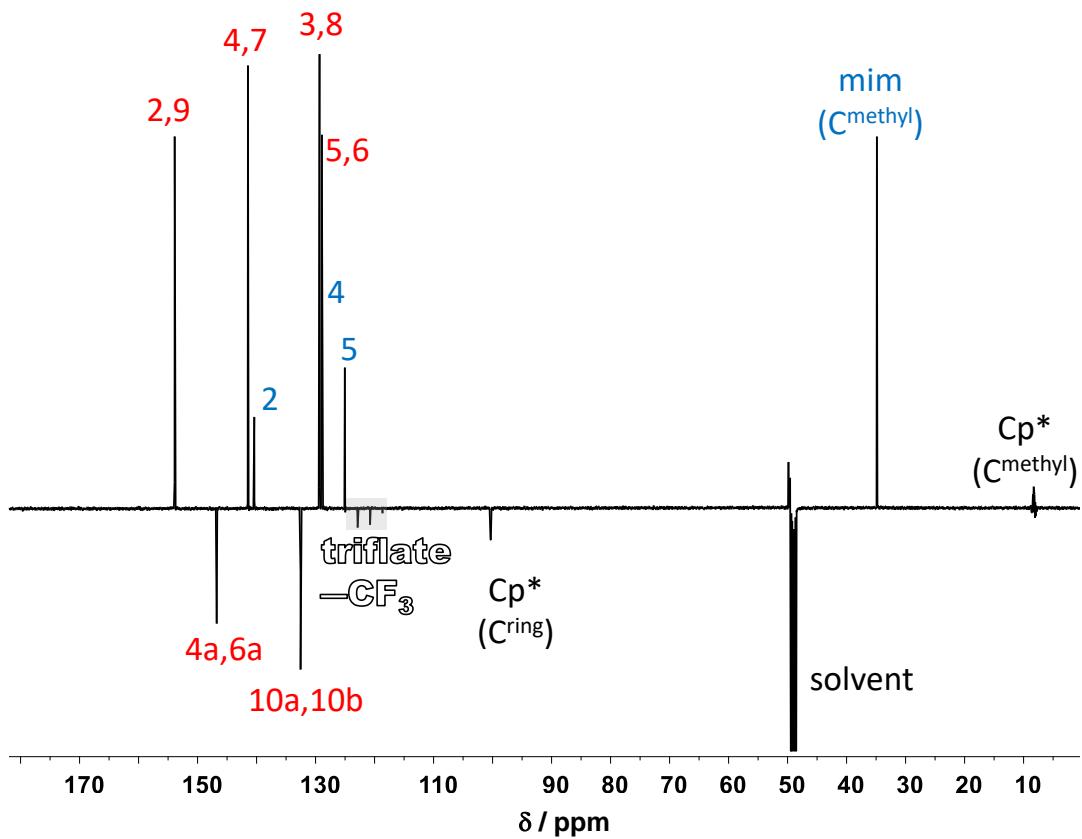
Figure S7. ^{13}C APT NMR spectrum of [RhCp*(phen)(mim)](CF$_3$SO$_3$)$_2$ in CD$_3$OD. For numbering see **Figure S6**. {c(complex) = 10 mM, t = 25.0°C}
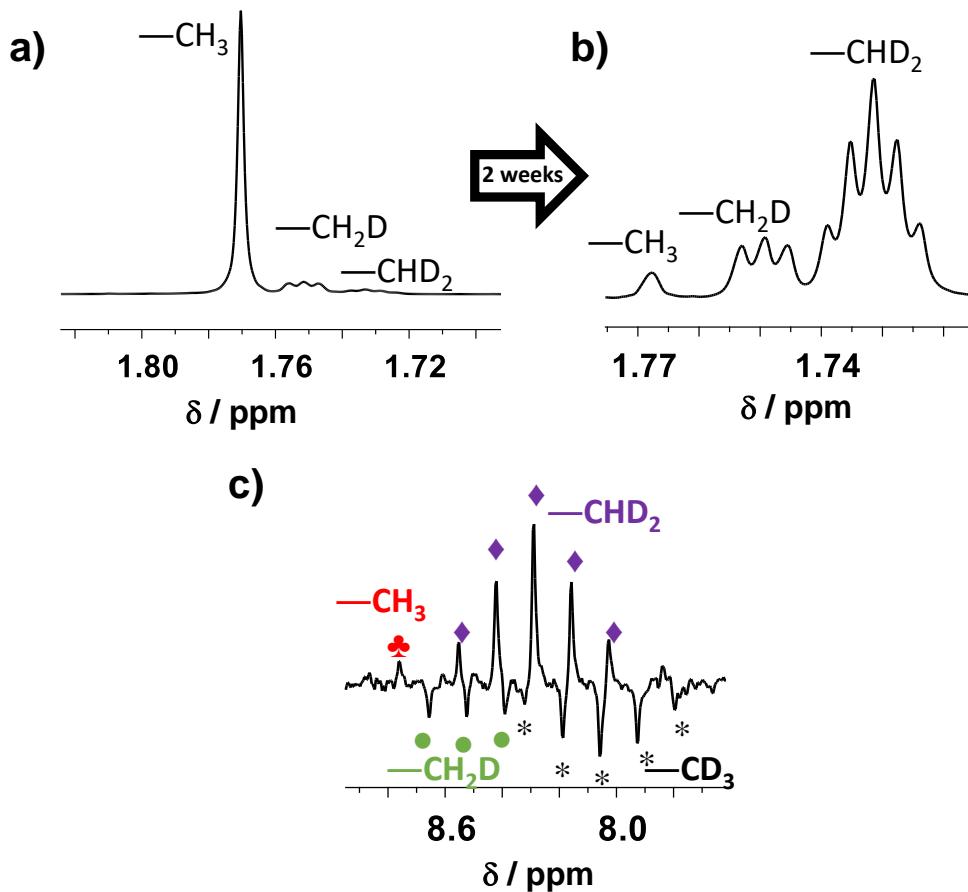
Figure S8. Upfield region of the ^1H NMR spectrum of $[RhCp*(phen)(mim)](CF_3SO_3)_2$ in CD_3OD. a) Freshly prepared sample (waiting time < 1 day prior to measurement) and b) after ~2 weeks. c) Upfield region of the compound's ^{13}C NMR spectrum shows the presence of the **Cp*** methyl groups at different deuterated stages measured 2-week-old sample. {c(complex) = 10 mM, t = 25.0°C}

9
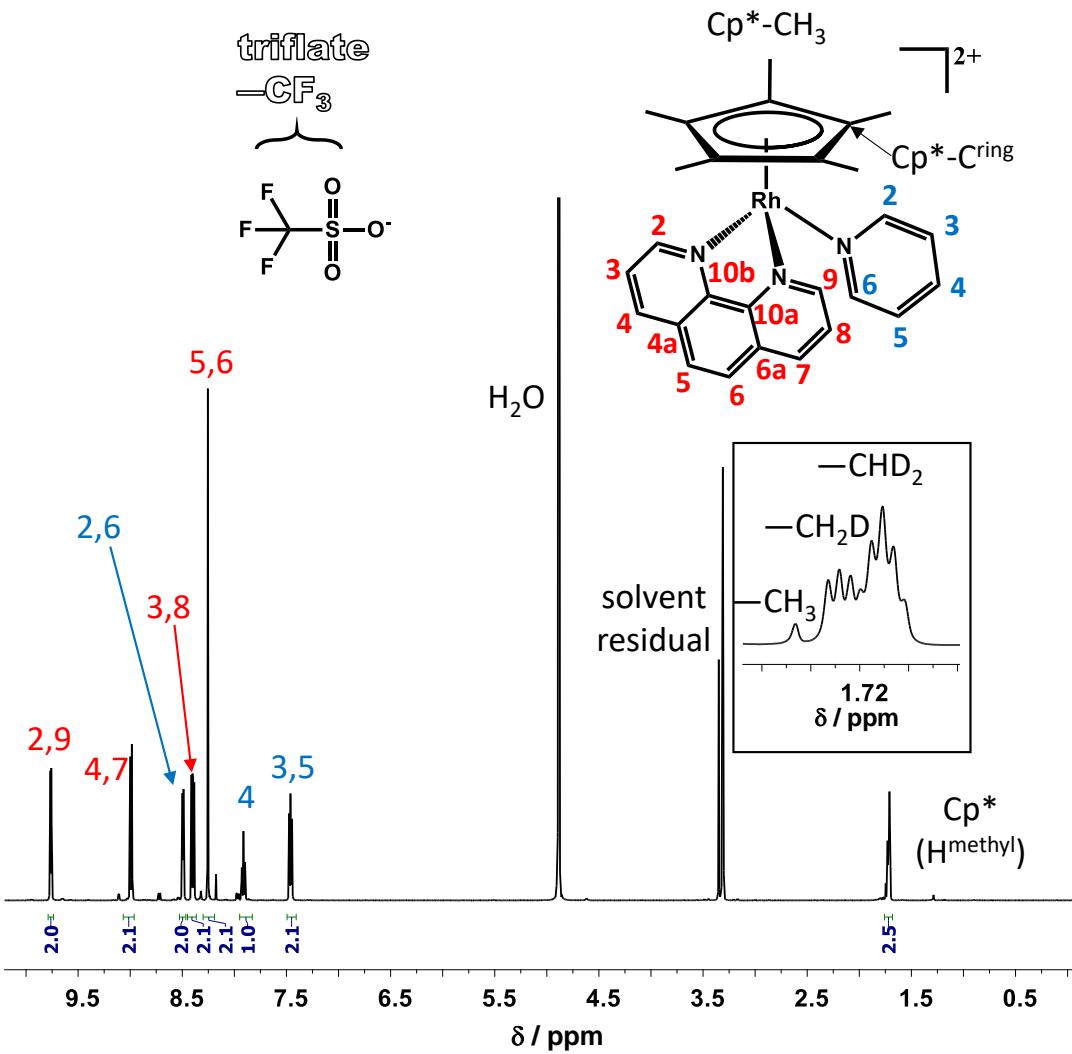
Figure S9. ^{1}H NMR spectrum of [RhCp*(phen)(Py)](CF₃SO₃)₂ in CD₃OD. Inserted structure shows numbering of peaks. Inset shows the methyl groups of **Cp*** at different deuteration stages. {c(complex) = 10 mM, t = 25.0°C}

Figure S10. ^{13}C APT NMR spectrum of [RhCp*(phen)(Py)](CF$_3$SO$_3$)$_2$ in CD$_3$OD. For numbering see **Figure S9**. Inset shows the presence of the **Cp*** methyl groups at different deuterated stages. {c(complex) = 10 mM, t = 25.0°C}
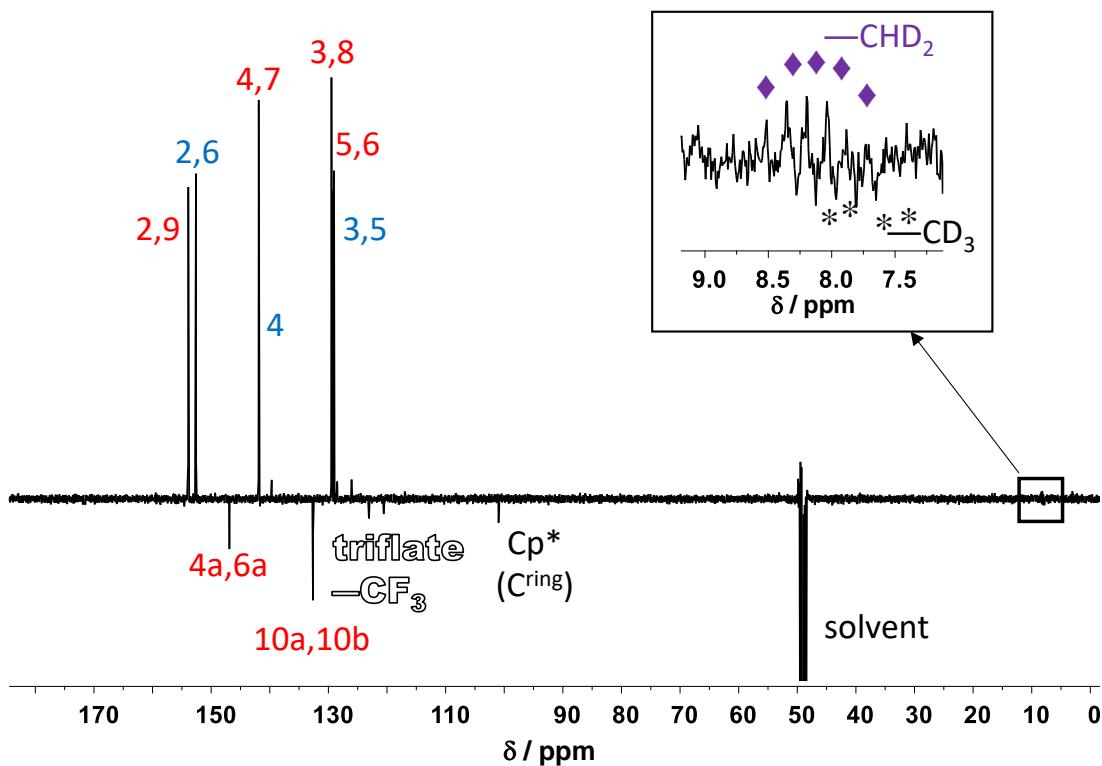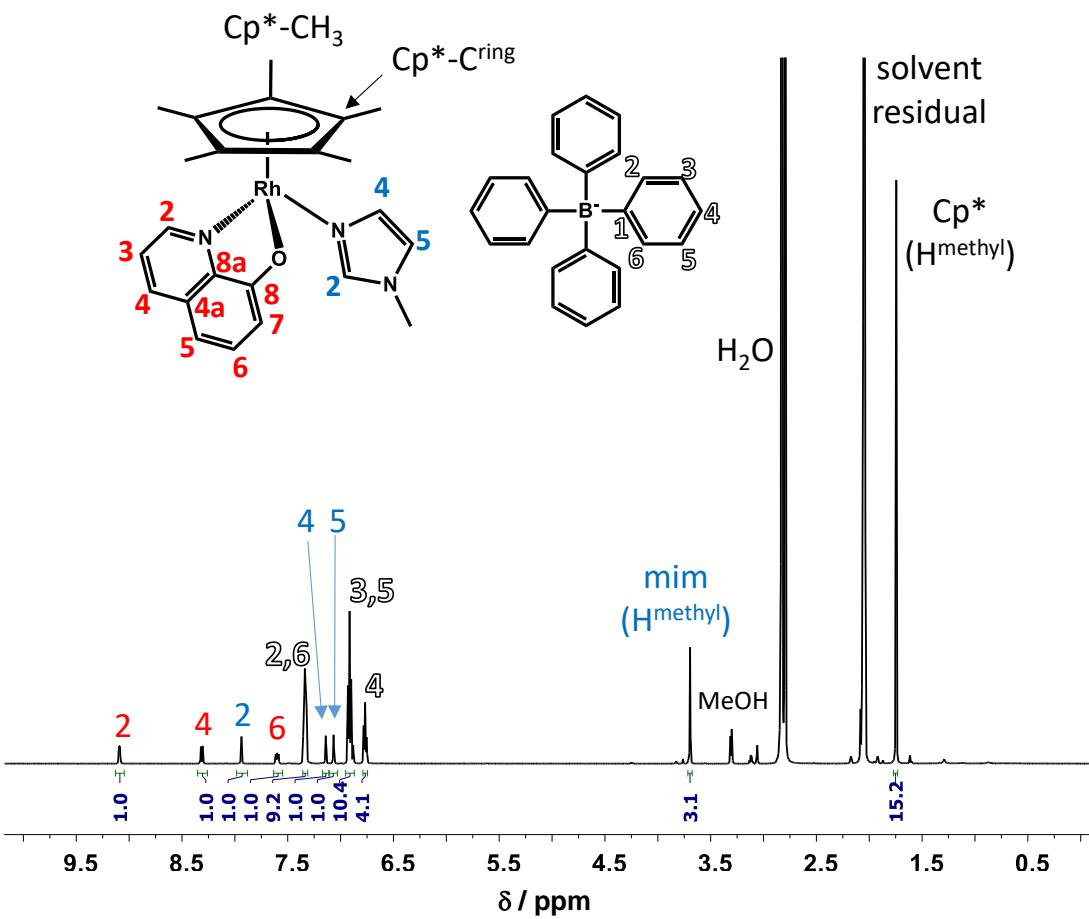
Figure S11. ^{1}H NMR spectrum of [RhCp*(8HQH$_{-1}$)(mim)](BPh$_4$) in acetone-d$_6$. Inserted structure shows numbering of peaks. {c(complex) = 2 mM, t = 25.0°C}
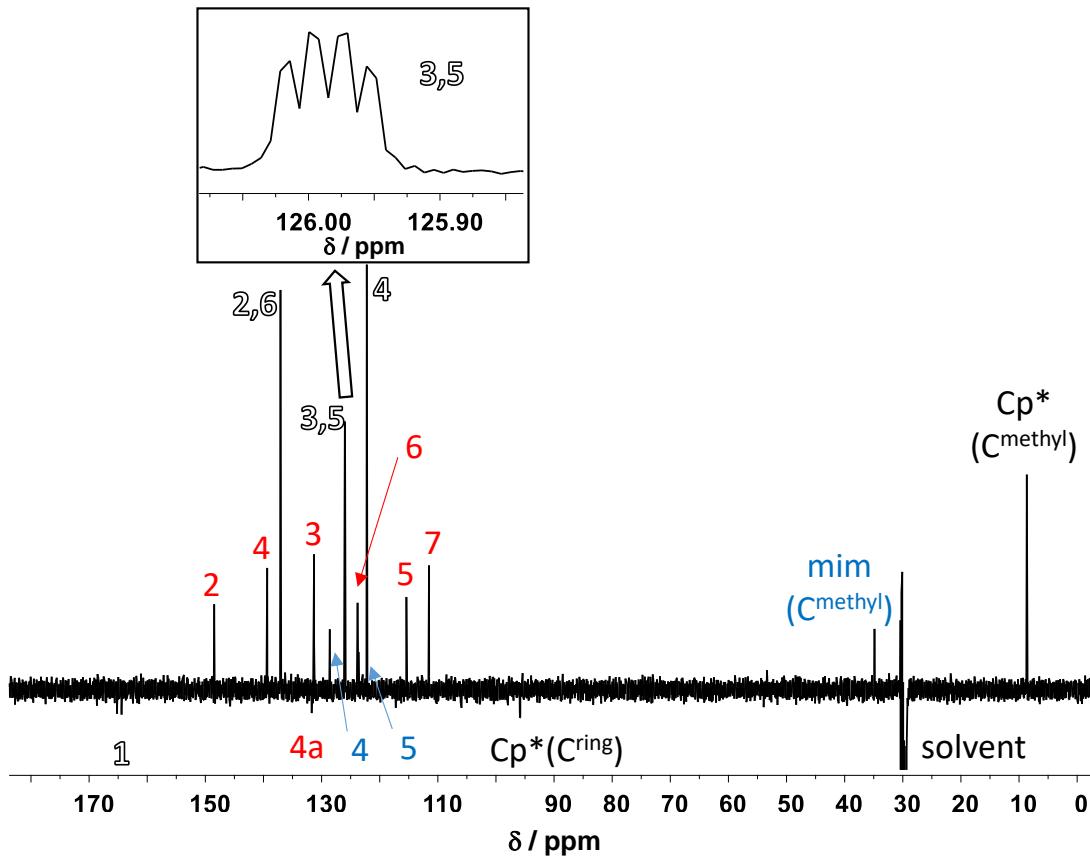
Figure S12. ^{13}C APT NMR spectrum of [RhCp*(8HQH$_{-1}$)(mim)](BPh$_4$) in acetone-d$_6$. For numbering see **Figure S11**. Inset shows the coupling with ^{11}B in BPh$_4^-$. {c(complex) = 2 mM, t = 25.0°C}
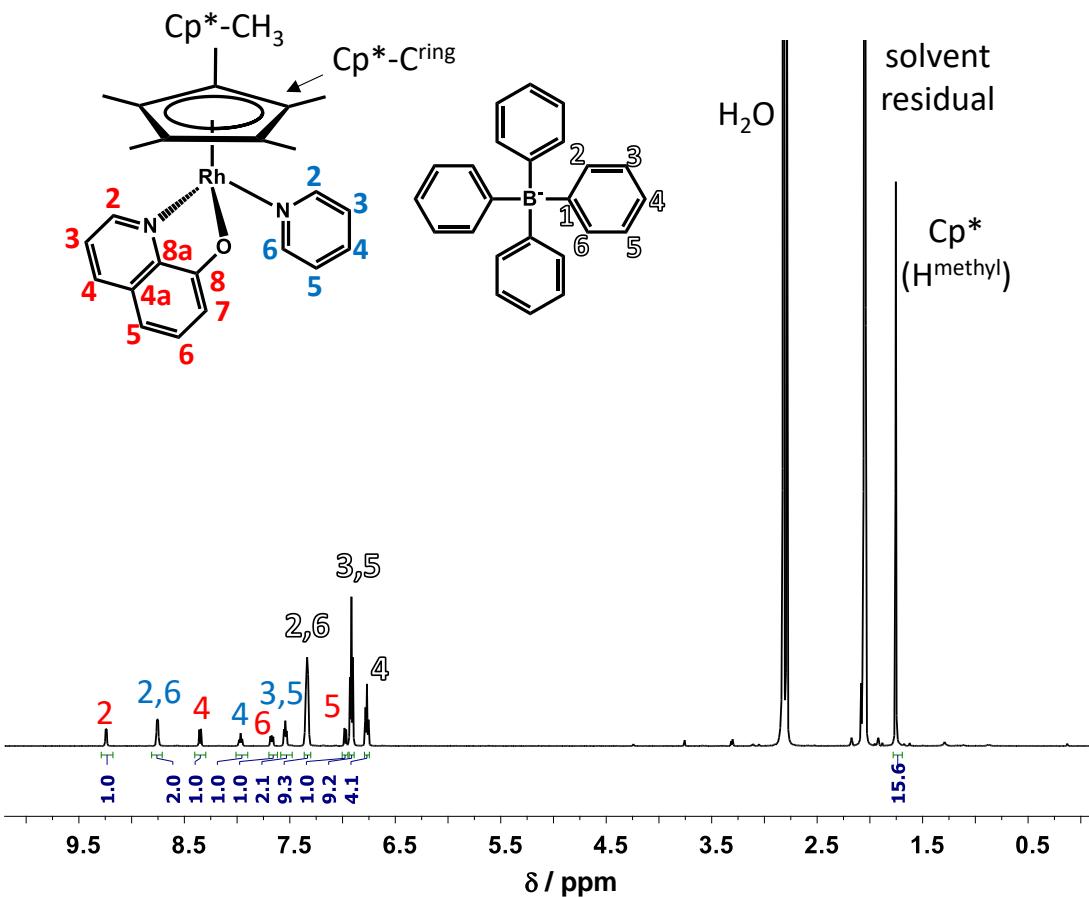
Figure S13. ^{1}H NMR spectrum of [RhCp*(8HQH$_{-1}$)(Py)](BPh$_4$) in acetone-d$_6$. Inserted structure shows numbering of peaks. {c(complex) = 2 mM, t = 25.0°C}
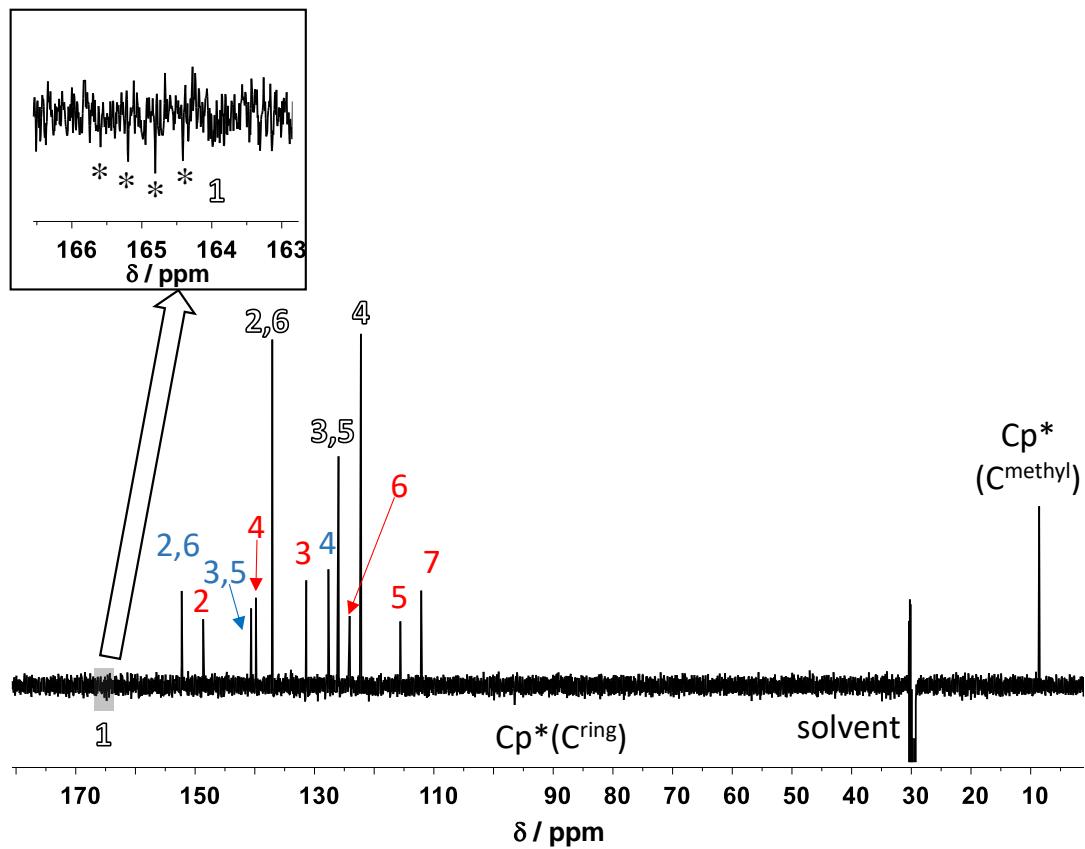
Figure S14. ^{13}C APT NMR spectrum of [RhCp*(8HQH$_{-1}$)(Py)](BPh$_4$) in acetone-d$_6$. For numbering see **Figure S13**. Inset shows the coupling with ^{11}B in BPh$_4^-$. {c(complex) = 2 mM, t = 25.0°C}

15

DATA QUALITY OF STRUCTURE DETERMINATION, COMPARISON OF M–N BOND LENGTHS
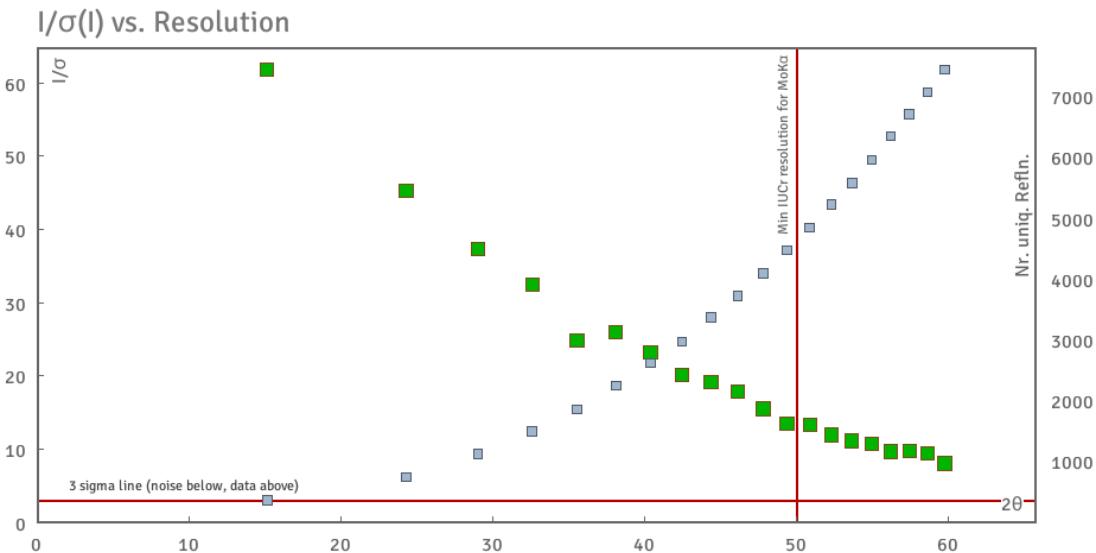
Figure S15. Data quality for complex **1′**: all data are above the three sigma line (along the minimum defined by the International Union of Crystallography (IUCR)).
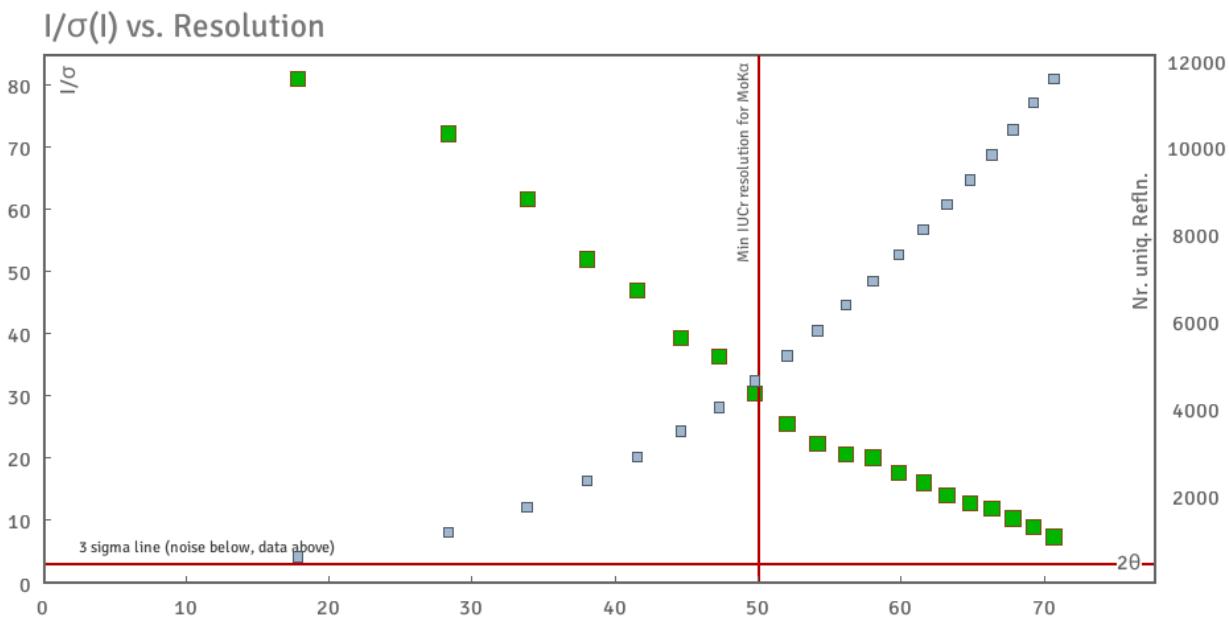
Figure S16. Data quality for complex **2′**: all data are above the three sigma line (along the minimum defined by IUCR).
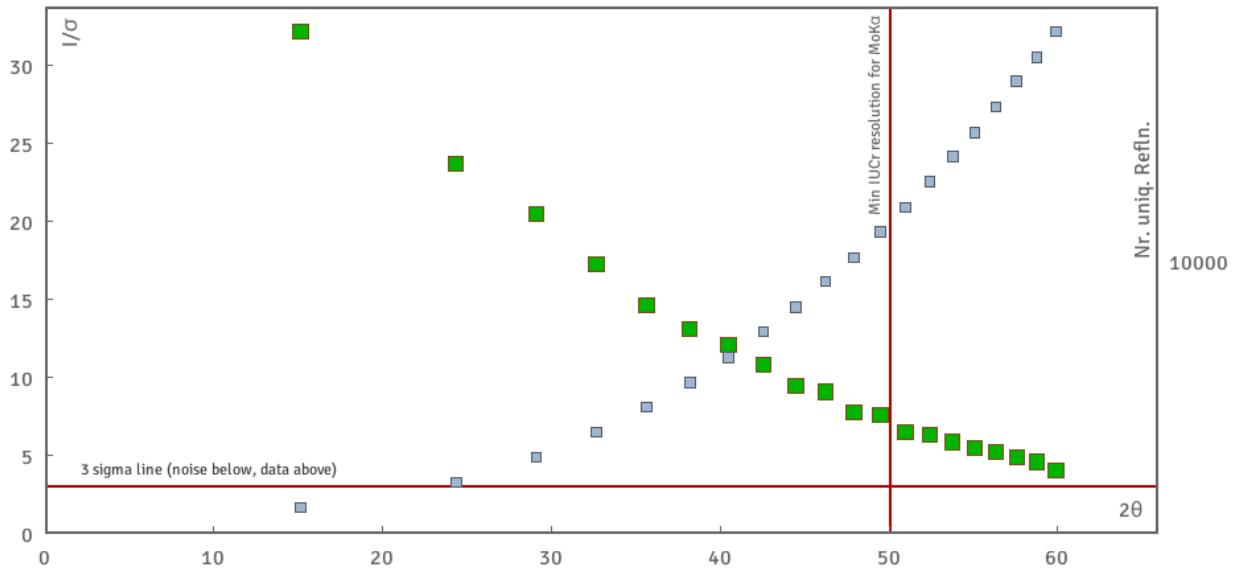
Figure S17. Data quality for complex **3′**: all data are above the three sigma line (along the minimum defined by IUCR).
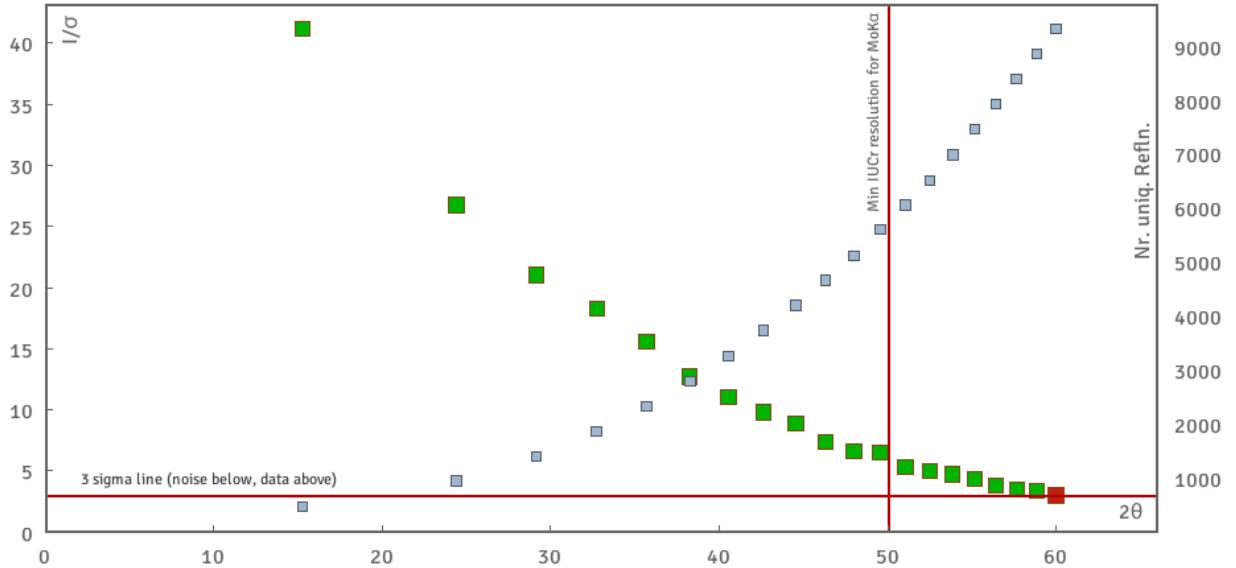
Figure S18. Data quality for complex **4′**: all data are above the three sigma line (along the minimum defined by IUCR).
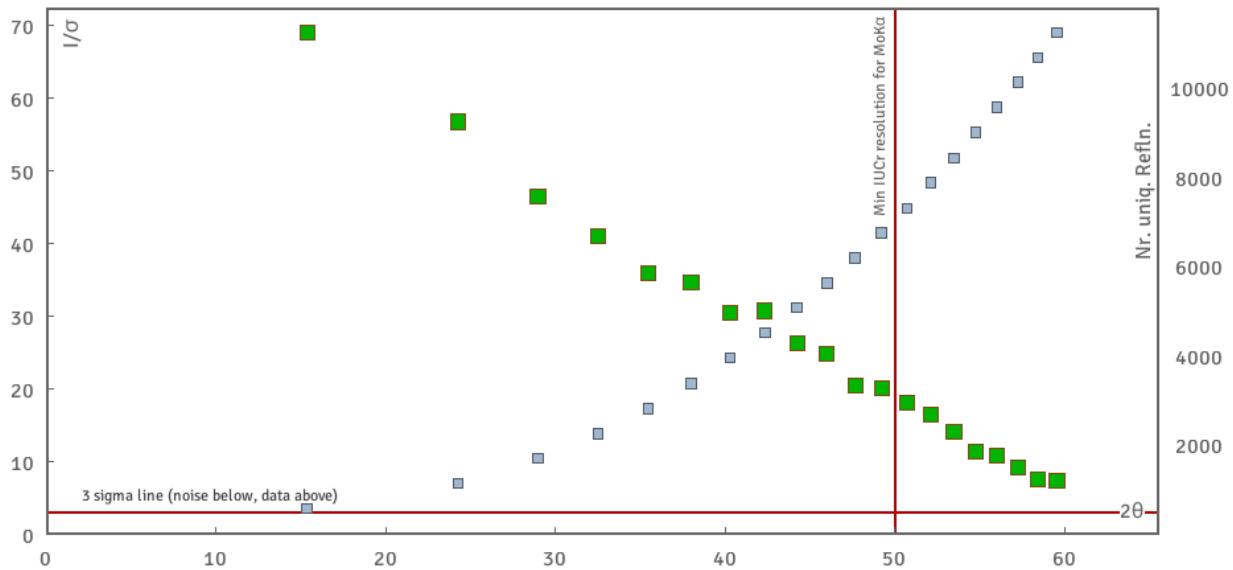
Figure S19. Data quality for complex **5'**: all data are above the three sigma line (along the minimum defined by IUCR).
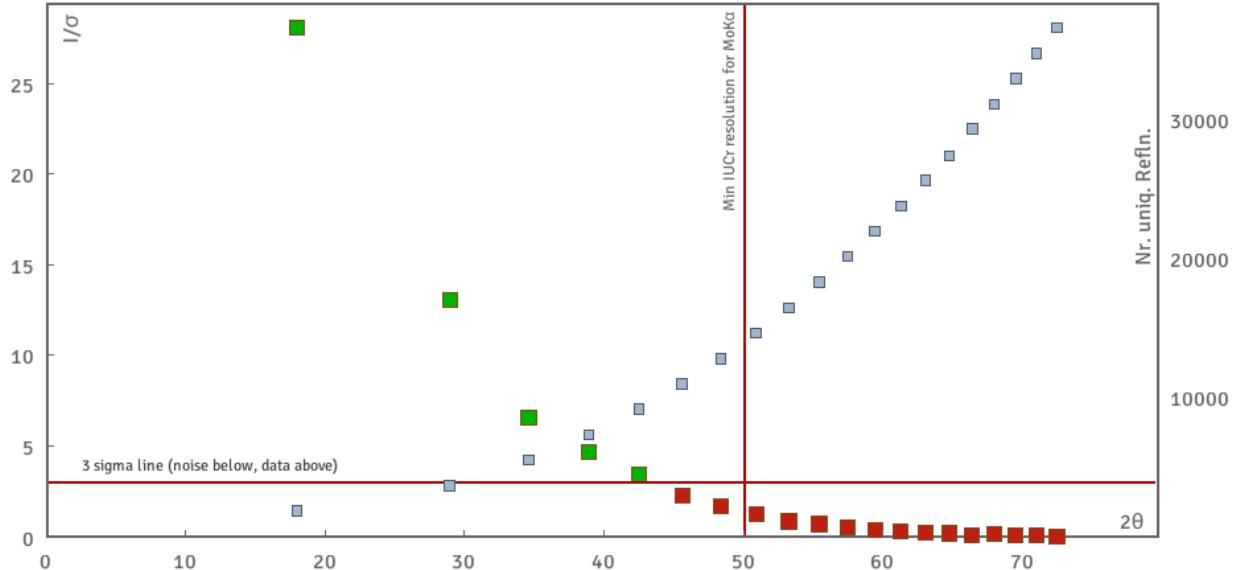
Figure S20. Data quality for complex **6'**: almost all data are above the three sigma line (along the minimum defined by IUCR). Data close to 50 degree (0.82, Mo) are still used in the refinement.

UV-Vis SPECTRA, FRACTIONS OF MIXED-LIGAND COMPLEXES AS THE FUNCTION OF pH, COMPARISON OF M–N BOND LENGTHS
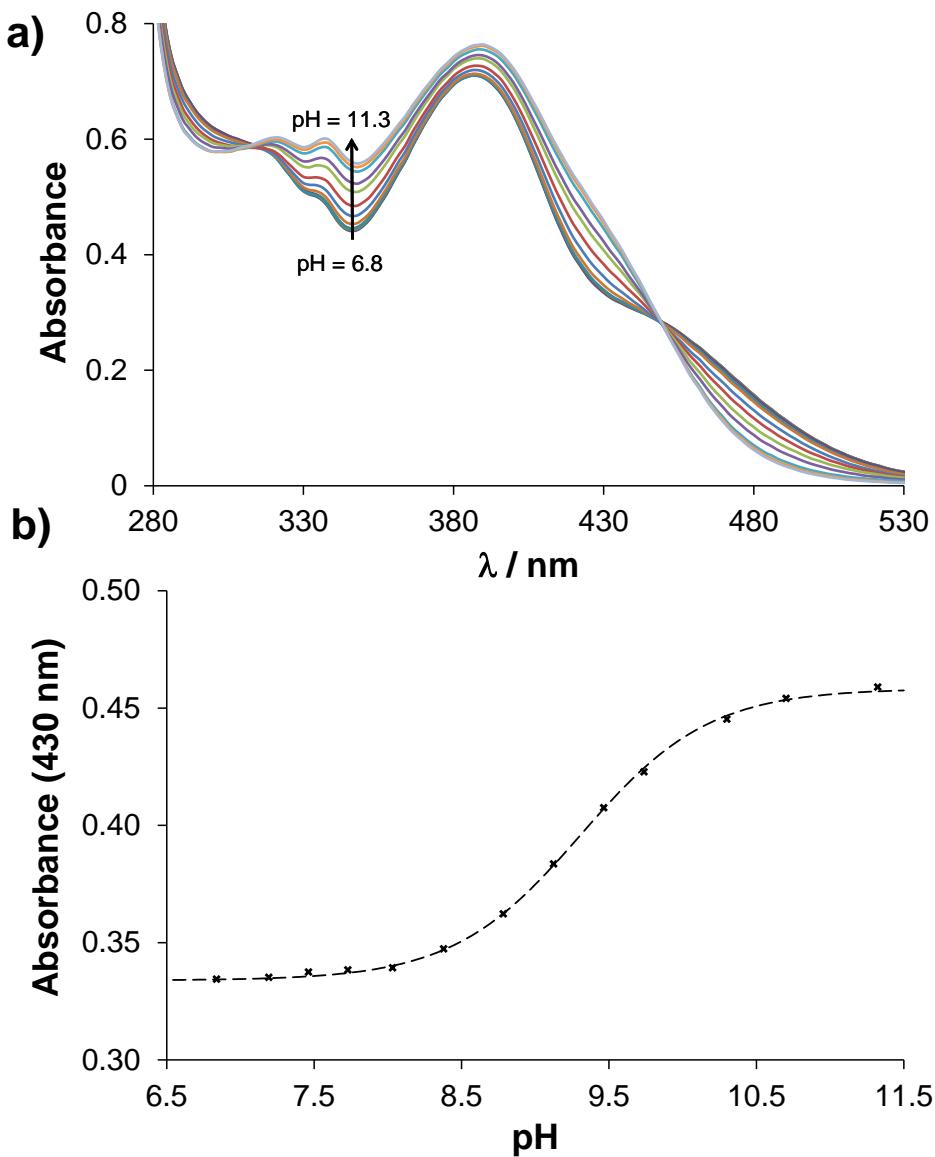
Figure S21. a) pH-dependent UV-vis spectra of $[Ru(\eta^6\text{-}p\text{-cym})(8HQH_{-1})(H_2O)]^+$ in the pH-range 2.0–11.5. b) Absorbance values at 430 nm in the function of pH. $\{c([Ru(\eta^6\text{-}p\text{-cym})(8HQH_{-1})(H_2O)]^+) = 200\ \mu M;\ I = 0.10\ M\ (KCl),\ t = 25\ °C,\ \ell = 1\ cm\}$
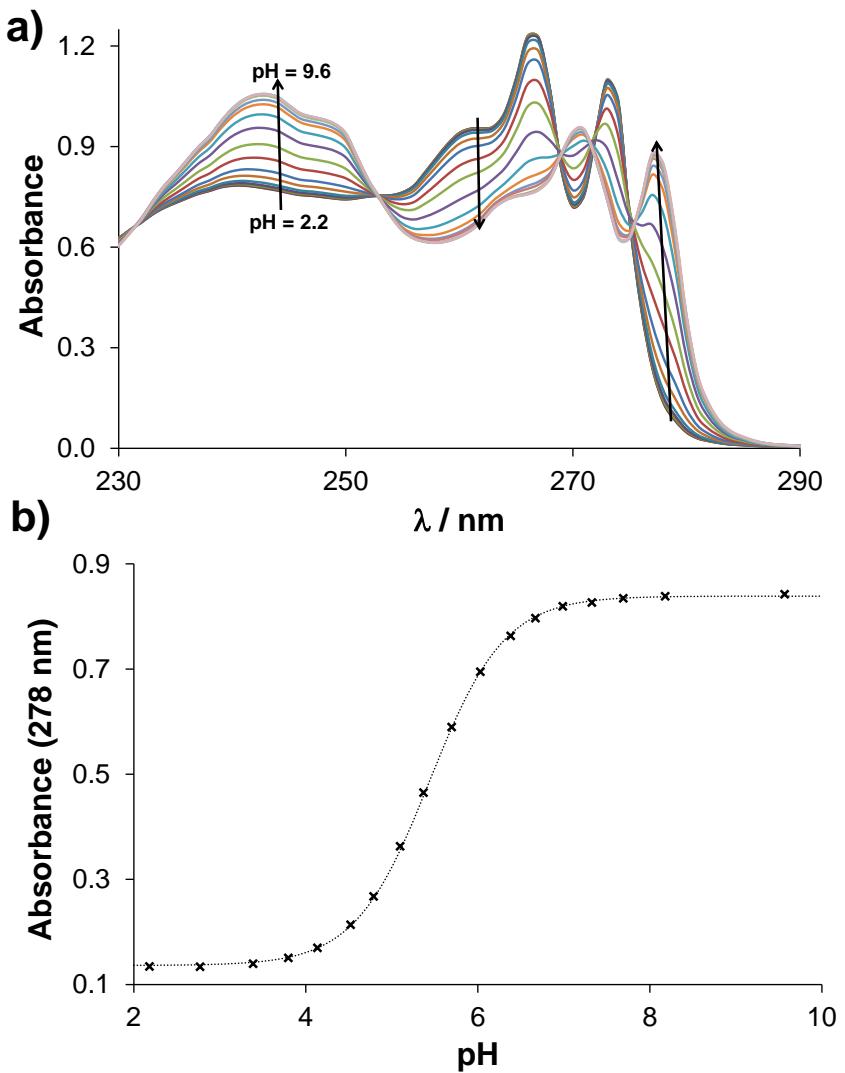
Figure S22. a) pH-dependent UV-vis spectra of benzimidazole in the pH-range 2.0–10.5. b) Absorbance values at 278 nm in the function of pH together with the fitted line (dotted line). {c(bim) = 200 µM; I = 0.10 M (KCl), t = 25 °C, ℓ = 0.2 cm}.
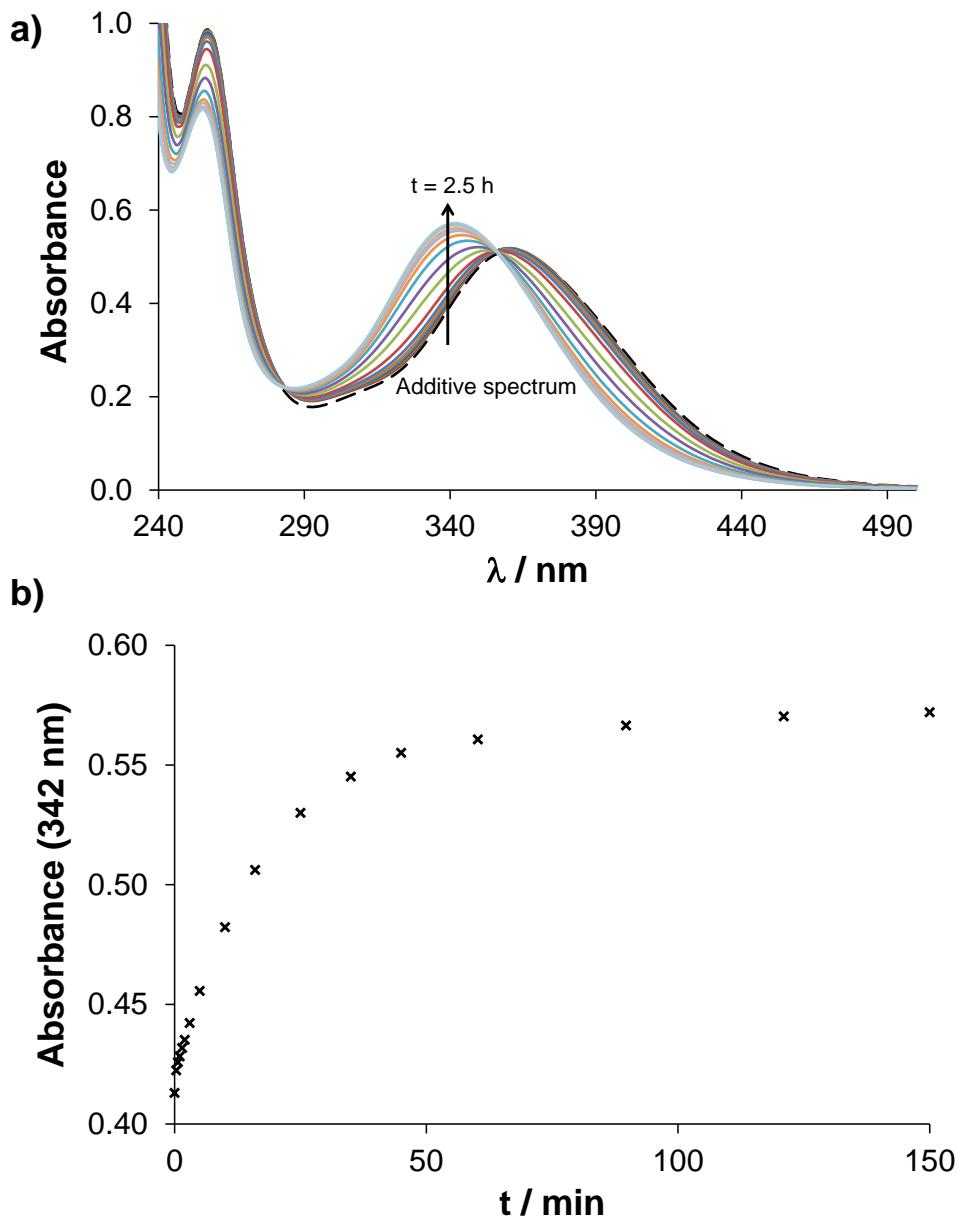
Figure S23. a) Time-dependent UV-vis spectra of the sample containing a mixture with $c([RhCp^*(en)(H_2O)]^{2+}):c(1\text{-methylimidazole}) = 1:2$ composition at pH = 5.94. b) Time dependence of absorbance values at 342 nm. $\{c([RhCp^*(en)(H_2O)]^{2+}) = 200\ \mu M;\ c(1\text{-methylimidazole}) = 400\ \mu M;\ pH = 5.94\ (PBS');\ t = 25\ °C;\ \ell = 1\ cm\}$
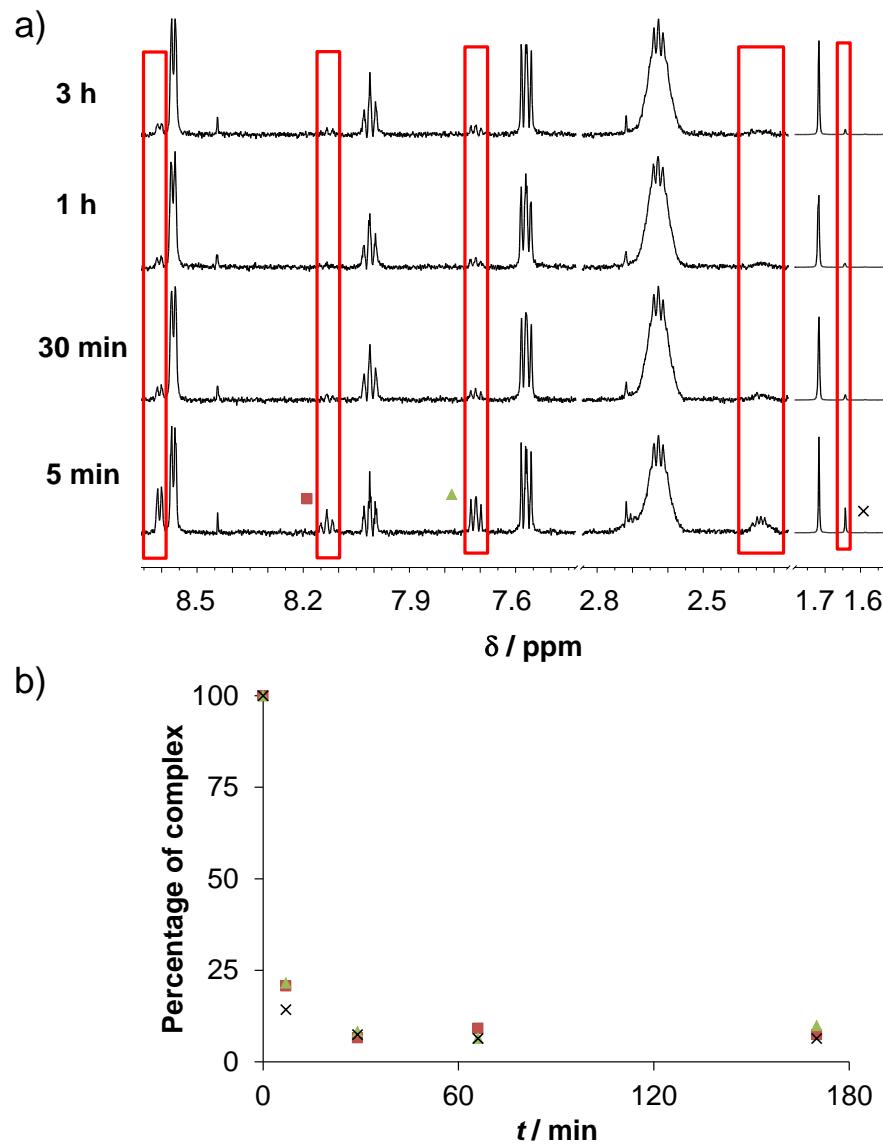
Figure S24. a) Time-dependent ^1H NMR spectra of the $[RhCp^*(en)(Py)](CF_3SO_3)_2$ synthesized complex at pH = 6.0. Red rectangles are highlighting peaks of the remaining mixed-ligand complex. b) Time-dependence of the presence of mixed-ligand complex (in percentage) based on integrals of the peaks of pyridine and Cp*. Assignation: × = Cp*; ■ = pyr-$H^{3,5}$; ▲ = pyr-H^4. {$c([RhCp^*(en)(Py)](CF_3SO_3)_2)$ = 200 μM; pH = 6.0 (PBS'); 10% D_2O; t = 25 °C; }
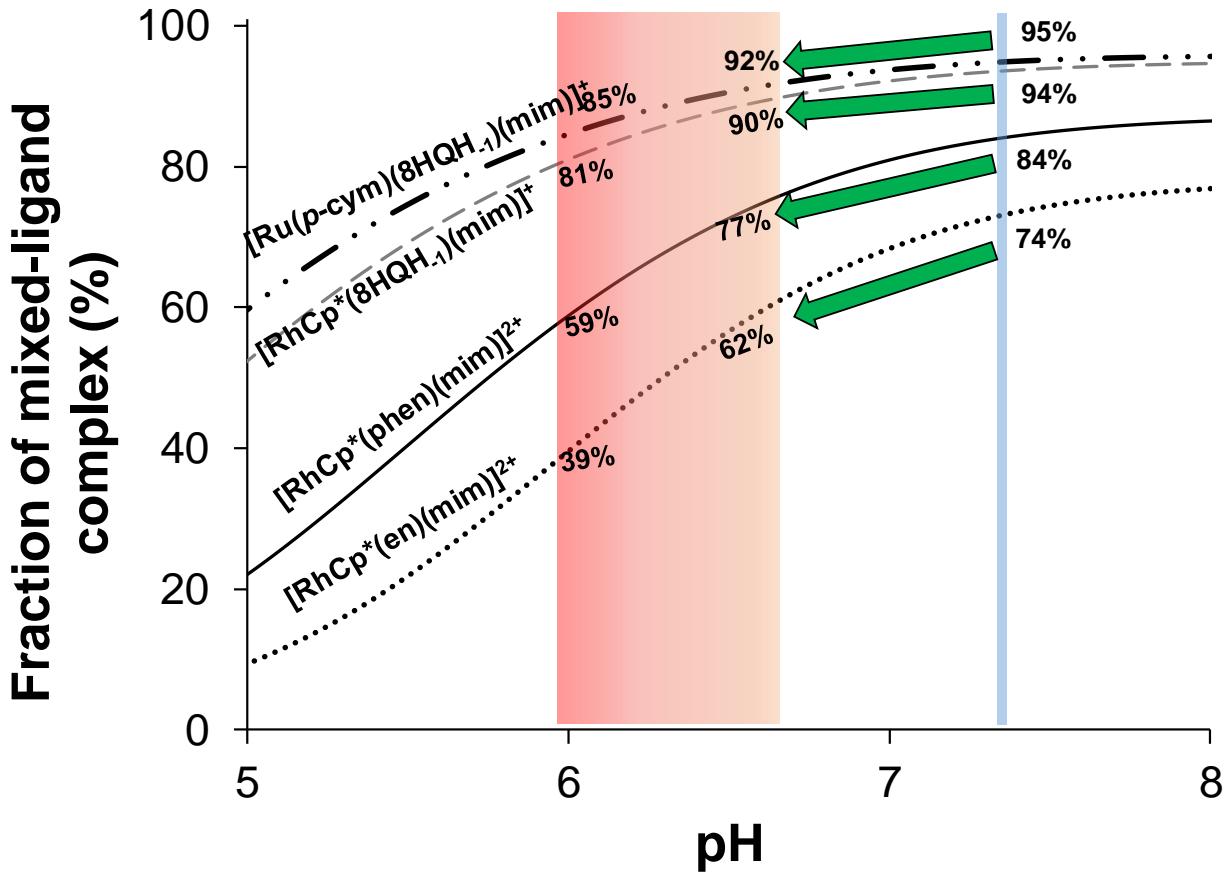
Figure S25. Fractions of the formed mixed-ligand complexes of 1-methylimidazole in the pH-range 5.0–8.0. Calculations based on the stability constants of the mixed-ligand complexes (**Table S2**) and proton dissociation constants in **Table 1**. {c([M(arene)(N,N/O)(H$_2$O)) = c(mim) = 100 μM; I = 0.10 M (KCl), t = 25 °C}.
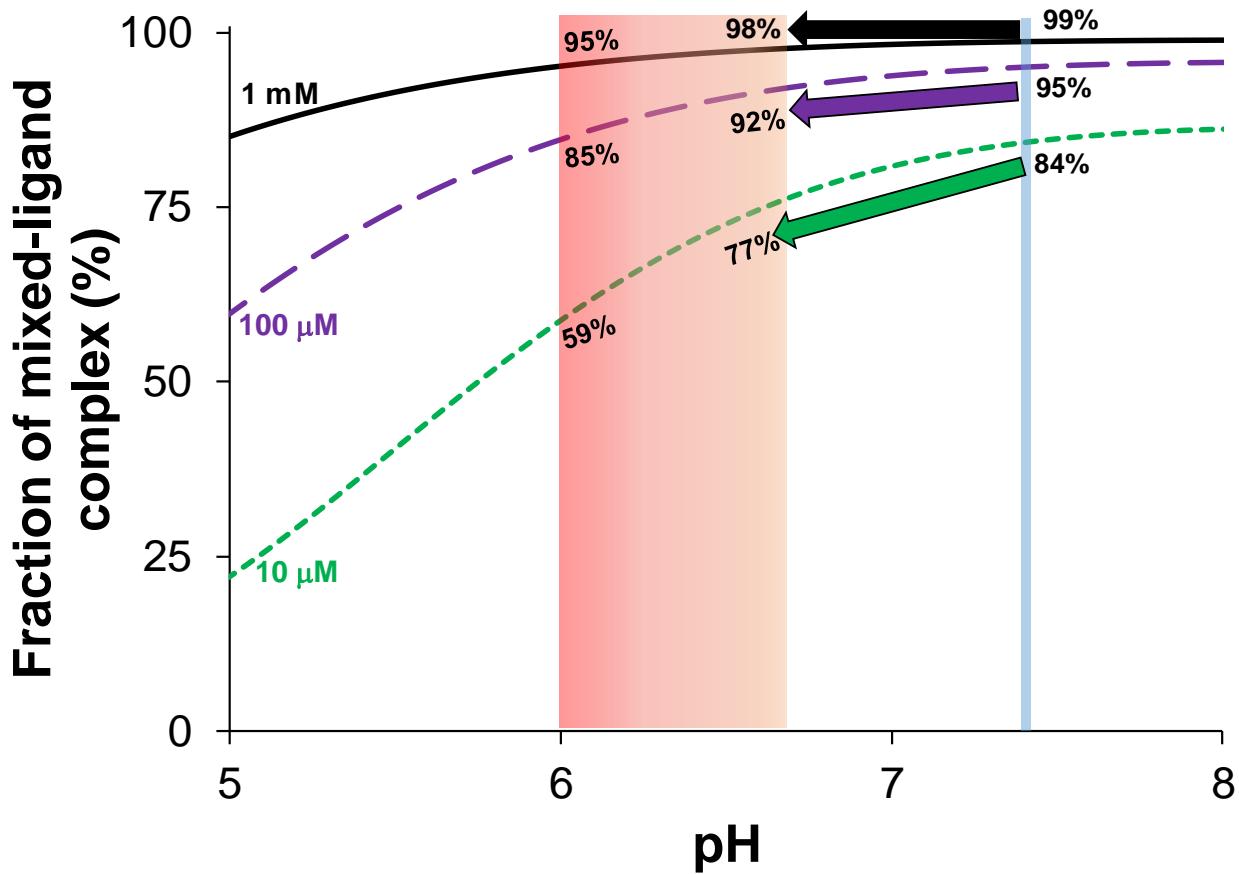
Figure S26. Formation (%) of [Ru(η^6-*p*-cym)(8HQH$_{-1}$)(mim)]$^+$ in the pH-range 5.0–8.0 at various equimolar concentrations of monodentate ligand and aqua complex. {c([Ru(η^6-*p*-cym)(8HQH$_{-1}$)(H$_2$O)]$^+$) = c(mim) = 10 μM, 100 μM or 1 mM; I = 0.10 M (KCl), t = 25 °C}.
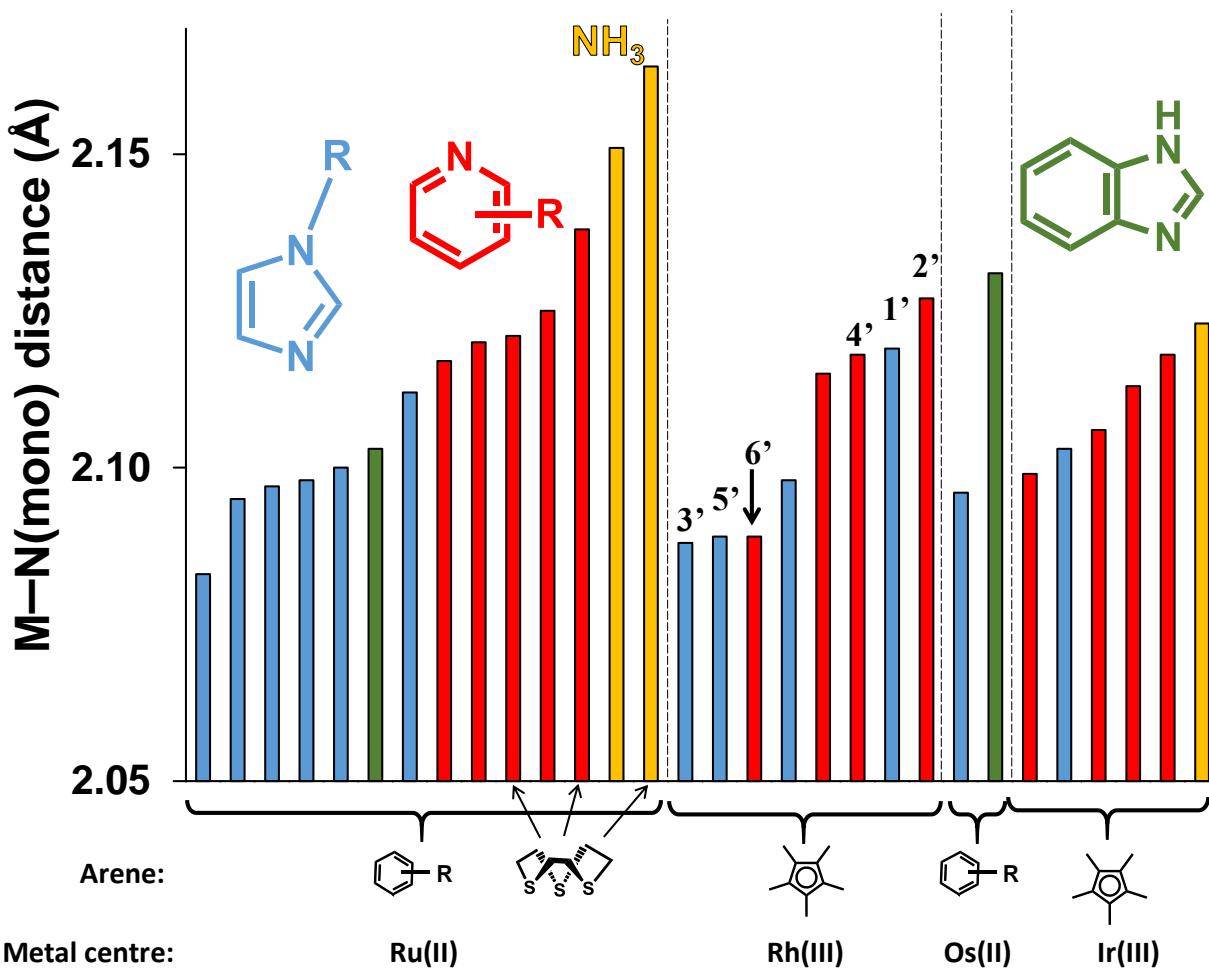
Figure S27. Comparison of the M–N(monodentate) distances in different [M(arene)(N,N/O)(N)]-type complexes reported in references [1-12]. Colour code for the monodentate ligand: blue: imidazole derivatives; red: pyridine derivatives; green: benzimidazole; yellow: NH_3. Roman numbers indicate the values derived from complexes **1'–6'**.

TABLES: PROTON DISSOCIATION CONSTANTS AND FORMATION CONSTANTS

Table S1. Proton dissociation constants of the coordinated water molecules in $[M(arene)(N,N/O)(H_2O)]^{2+/+}$ complexes {$I = 0.10$ M (KCl); $t = 25.0$ °C}.

Compound	pK_a	Method	Literature data
$[RhCp^*(en)(H_2O)]^{2+}$	10.6±0.1	UV-vis	9.58[1] [13]
			11.05[2] [13]
$[RhCp^*(8HQH_{-1})(H_2O)]^+$	10.6±0.1	UV-vis	10.27[2] [14]
$[RhCp^*(phen)(H_2O)]^{2+}$	10.05±0.01	UV-vis	8.58[2] [15]
$[Ru(p\text{-cym})(en)(H_2O)]^{2+}$	9.03±0.01	UV-vis	8.14[2] [15]
$[Ru(p\text{-cym})(8HQH_{-1})(H_2O)]^+$	9.31±0.01	UV-vis	9.19[2] [14]
$[Ru(p\text{-cym})(phen)(H_2O)]^{2+}$	8.91±0.01	UV-vis	7.59[2] [15]

[1] $I = 0.20$ M (KNO$_3$); [2] $I = 0.20$ M (KCl)

Table S2. Formation constants (log$K$) determined for mixed-ligand half-sandwich complexes of Rh(III) and Ru(II) by UV-vis and ^{1}H NMR spectroscopy {$I = 0.10$ M (KCl); $t = 25.0$ °C}.

$$[M(arene)(N,N/O)(H_2O)]^{2+/+} + N_{mono} \rightleftharpoons [M(arene)(N,N/O)(N_{mono})]^{2+/+} + H_2O$$
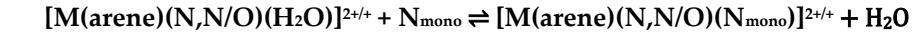
Aqua complex	Monodentate ligand	log$K$
$[RhCp^*(en)(H_2O)]^{2+}$	bim	3.3 ± 0.2
$[RhCp^*(en)(H_2O)]^{2+}$	mim	4.2 ± 0.1
$[RhCp^*(en)(H_2O)]^{2+}$	Py	2.6 ± 0.1
$[RhCp^*(phen)(H_2O)]^{2+}$	bim	4.9 ± 0.2
$[RhCp^*(phen)(H_2O)]^{2+}$	mim	5.5 ± 0.1
$[RhCp^*(phen)(H_2O)]^{2+}$	Py	4.1 ± 0.1
$[RhCp^*(8HQH_{-1})(H_2O)]^+$	bim	3.4 ± 0.1
$[RhCp^*(8HQH_{-1})(H_2O)]^+$	mim	4.7 ± 0.2
$[RhCp^*(8HQH_{-1})(H_2O)]^+$	Py	3.0 ± 0.1
$[RuCym(en)(H_2O)]^{2+}$	bim	3.5 ± 0.1
$[RuCym(en)(H_2O)]^{2+}$	mim	< 2.6
$[RuCym(en)(H_2O)]^{2+}$	Py	< 1.5
$[RuCym(phen)(H_2O)]^{2+}$	bim	5.6 ± 0.2
$[RuCym(phen)(H_2O)]^{2+}$	mim	6.7 ± 0.2
$[RuCym(phen)(H_2O)]^{2+}$	Py	4.3 ± 0.2
$[RuCym(8HQH_{-1})(H_2O)]^+$	bim	2.9 ± 0.1
$[RuCym(8HQH_{-1})(H_2O)]^+$	mim	< 2.6
$[RuCym(8HQH_{-1})(H_2O)]^+$	Py	1.6 ± 0.2

EXPERIMENTAL DATA TABLES FOR SINGLE-CRYSTAL XRD

Table S3. Experimental parameters for the single crystal X-ray diffraction data collection and CCDC-code of the synthesized complexes.

CCDC-code	Sample	Machine	Source	Temp.	Detector Distance	Time/ Frame	Frames	Frame width
				[K]	[mm]	[s]		[°]
2209815	6′	Stoe Stadivari	Mo	100	40	10	1804	0.5
2209816	4′	Bruker X8	Mo	100	36	6	1347	0.5
2209817	2′	Bruker D8	Mo	100	34	6	1805	0.5
2209818	3′	Bruker X8	Mo	100	40	8.1	5595	0.5
2209819	1′	Bruker X8	Mo	100	35	7	833	0.6
2209820	5′	Bruker D8	Mo	100	35	3	1390	0.6

Table S4. Crystal data and structure refinement for complexes **1'-3'**.

	1'	2'	3'
Empirical formula	$C_{18}H_{29}F_6N_4O_6RhS_2$	$C_{19}H_{28}F_6N_3O_6RhS_2$	$C_{76}H_{73}B_2Cl_4N_4Rh$
Formula weight	678.48	675.47	1308.71
Temperature (K)	100.0	100.0	100.0
Crystal system, Space group	triclinic	triclinic	triclinic
Space group	P-1	P-1	P-1
Unit cell dimensions			
a (Å)	7.7751(4)	7.8309(4)	12.9421(9)
b (Å)	11.5350(7)	10.8399(5)	12.9452(9)
c (Å)	15.4437(9)	15.7969(7)	20.0369(13)
α (°)	100.4691(17)	89.5353(16)	76.964(3)
β (°)	91.3163(17)	85.0745(16)	85.322(3)
γ (°)	103.4897(17)	79.0821(16)	86.772(4)
Volume (Å^3)	1321.35(13)	1311.76(11)	3255.8(4)
Z	2	2	2
ϱ_{calc} (g/cm^3)	1.705	1.710	1.335
μ (mm^{-1})	0.887	0.892	0.474
F(000)	688.0	684.0	1360.0
Crystal size (mm)	0.13×0.1× 0.07	0.423×0.227×0.08	0.3×0.11×0.08
Radiation	Mo-K$_\alpha$ (λ=0.71073 Å)		
2Θ range for data collection (°)	5.378-54.206	4.602-71.378	4.432-50.7
Index ranges	-9≤h≤9, -14≤k≤14, -19≤l≤19	-12≤h≤12, -17≤k≤17, -25≤l≤23	-15≤h≤15, -15≤k≤15, -23≤l≤24
Reflections collected	14736	58577	97481
Independent reflections	5816 [R_{int}=0.0269, R_{sigma}=0.0308]	12115 [R_{int}=0.0303, R_{sigma}=0.0271]	11943 [R_{int}=0.0804, R_{sigma}=0.0482]
Data / restraints / parameters	5816 /36 /364	12115 / 0 / 339	11943 / 0 / 790
Goodness-of-fit on F^2	1.030	1.073	1.089
Final R indices [I>2$\sigma(I)$]	R_1=0.0331, wR_2=0.0788	R_1=0.0265, wR_2=0.0571	R_1=0.0452, wR_2=0.1179
R indices (all data)	R_1=0.0361, wR_2=0.0809	R_1=0.0328, wR_2=0.0592	R_1=0.0501, wR_2=0.1220
Largest diff. peak and hole (e×Å^{-3})	1.64 / -1.04	0.95 / -1.08	1.50 / -1.67

Table S5. Crystal data and structure refinement for complexes **4′-6′**.

	4′	5′	6′
Empirical formula	$C_{30}H_{32}F_6N_3O_7RhS_2$	$C_{48}H_{51}BN_3O_2Rh$	$C_{48}H_{46}BN_2ORh$
Formula weight	827.61	815.64	780.59
Temperature (K)	100.0	100.0	100.0
Crystal system, Space group	monoclinic	monoclinic	monoclinic
Space group	$P2_1/c$	$P2_1/n$	$P2_1/c$
Unit cell dimensions			
a (Å)	13.0591(11)	11.8020(5)	29.1880(10)
b (Å)	13.5115(9)	27.8595(9)	11.8065(3)
c (Å)	18.9926(15)	12.2552(9)	24.8781(10)
α (°)	90	90	90
β (°)	102.252(3)	90.8912(11)	114.956(3)
γ (°)	90	90	90
Volume (Å³)	3274.9(4)	4029.0(4)	7772.7(5)
Z	4	4	8
ϱ_{calc} (g/cm³)	1.679	1.345	1.334
μ (mm⁻¹)	0.735	0.467	0.478
F(000)	1680.0	1704.0	3248.0
Crystal size (mm)	0.22×0.2×0.03	0.3×0.07×0.07	0.28×0.2×0.06
Radiation	Mo-K$_\alpha$ (λ=0.71073 Å)		
2Θ range for data collection (°)	3.728-50.69	4.524–60.092	3.274-51.364
Index ranges	-14≤h≤15, -15≤k≤16, -22≤l≤22	-16≤h≤16, -39≤k≤37, -17≤l≤17	-35≤h≤35, -14≤k≤14, -30≤l≤25
Reflections collected	28186	144915	83725
Independent reflections	5887 [R_{int}=0.0506, R_{sigma}=0.0447]	11780 [R_{int}=0.0628, R_{sigma}=0.0249]	14760 [R_{int}=0.1697, R_{sigma}=0.1700]
Data / restraints / parameters	5887 / 4 / 469	11780 / 0 / 504	14760 / 0 / 966
Goodness-of-fit on F^2	1.046	1.074	0.953
Final R indices [I>2σ(I)]	R_1=0.0442, wR_2=0.1065	R_1=0.0316, wR_2=0.0641	R_1=0.0661, wR_2=0.1492
R indices (all data)	R_1=0.0534, wR_2=0.1133	R_1=0.0404, wR_2=0.0697	R_1=0.1304, wR_2=0.1676
Largest diff. peak and hole (e×Å⁻³)	0.90 / -0.80	0.67 / -0.75	2.26 / -1.31

MIC VALUES FOR ALL COMPOUNDS, pH = 5–8

Table S6. Minimal inhibition concentration (MIC) (µM) of premixed complexes, bidentate and monodentate ligands on Gram-positive *S. aureus* bacterial strains after one day.

MIC (µM)	*S. aureus*, sensitive				*S. aureus*, resistant			
pH =	5	6	7	8	5	6	7	8
mim			>100	>100	>100	>100	>100	>100
Py			>100	>100	>100	>100	>100	>100
econ			0.78	0.19	25	12.5	6.25	3.125
zol			>100	>100	>100	>100	>100	>100
phen	Bacterial cell proliferation was inhibited	at that pH.	>100	>100	50	>100	>100	>100
8HQ			25	25	100	6.25	6.25	6.25
[RhCp*(phen)Cl]Cl			>100	>100	>100	>100	>100	>100
+mim			>100	>100	>100	>100	>100	>100
+Py			>100	>100	>100	>100	>100	>100
+econ			0.78	1.56	25	12.5	3.125	3.125
[RhCp*(8HQH₋₁)Cl]			12.5	12.5	50	12.5	12.5	12.5
+mim			12.5	12.5	50	25	12.5	12.5
+econ			0.39	0.39	12.5	6.25	3.125	3.125
+zol			12.5	25	50	50	12.5	12.5

Table S7. Minimal inhibition concentration (MIC) (µM) of premixed complexes, bidentate and monodentate ligands on Gram-negative *E. coli* bacterial strains after one day.

MIC (µM)	*E. coli*, sensitive				*E. coli*, resistant			
pH=	5	6	7	8	5	6	7	8
mim	>100	>100	>100	>100	>100	>100	>100	>100
Py	>100	>100	>100	>100	>100	>100	>100	>100
econ	>100	>100	>100	>100	>100	>100	>100	>100
zol	>100	>100	>100	>100	>100	>100	>100	>100
phen	50	50	50	25	50	50	50	50
8HQ	>100	>100	>100	>100	>100	>100	>100	>100
[RhCp*(phen)Cl]Cl	>100	>100	>100	>100	>100	>100	>100	>100
+mim	>100	>100	>100	>100	>100	>100	>100	>100
+Py	>100	>100	>100	>100	>100	>100	>100	>100
+econ	>100	>100	>100	>100	>100	>100	>100	>100
[RhCp*(8HQH₋₁)Cl]	>100	>100	>100	>100	>100	>100	>100	>100
+mim	>100	>100	>100	>100	>100	>100	>100	>100
+econ	25	25	25	25	50	100	100	50
+zol	>100	>100	>100	>100	>100	>100	>100	>100

REFERENCES

1. Wöckel, S.; Plessow, P.; Schelwies, M.; Brinks, M.K.; Rominger, F.; Hofmann, P.; Limbach, M. Alcohol Amination with Aminoacidato Cp*Ir(III)-Complexes as Catalysts: Dissociation of the Chelating Ligand during Initiation. *ACS Catal.* **2014**, *4*, 152–161. https://doi.org/10.1021/cs4009418

2. Babak, M.V.; Meier , S.M.; Legin, A.A.; Adib Razavi, M.S.; Roller, A.; Jakupec , M.A.; Keppler , B.K.; Hartinger, C.G. Am(m)ines Make the Difference: Organoruthenium Am(m)ine Complexes and Their Chemistry in Anticancer Drug Development. *Chem. Eur. J.* **2013**, *19*, 4308–4318. https://doi.org/10.1002/chem.201202657

3. Wang, F.; Habtemariam, A.; van der Geer, E.P.; Fernández, R.; Melchart, M.; Deeth, R.J.; Aird, R.; Guichard, S.; Fabbiani, F.P.; Lozano-Casal, P.; Oswald, I.D.; Jodrell, D.I.; Parsons, S.; Sadler, P.J. Controlling ligand substitution reactions of organometallic complexes: tuning cancer cell cytotoxicity. *Proc. Natl. Acad. Sci. U. S. A.* **2005**, *102*, 18269–18274. https://doi.org/10.1073/pnas.0505798102

4. Du, J.; Zhang, E.; Zhao, Y.; Zheng, W.; Zhang, Y.; Lin, Y.; Wang, Z.; Luo, Q.; Wu, K.; Wang, F. Discovery of a dual-targeting organometallic ruthenium complex with high activity inducing early stage apoptosis of cancer cells. *Metallomics* **2015**, *7* 1573–1583. https://doi.org/10.1039/C5MT00122F

5. Zhang, W.-Y.; Bridgewater, H.E.; Banerjee, S.; Soldevila-Barreda, J.J.; Clarkson, G.J.; Shi, H.; Imberti, C.; Sadler, P.J. Ligand-Controlled Reactivity and Cytotoxicity of Cyclometalated Rhodium(III) Complexes. *Eur. J. Inorg. Chem.* **2019**, *2020*, 1052–1060. https://doi.org/10.1002/ejic.201901055

6. Betanzos-Lara, S.; Salassa, L.; Habtemariam, A.; Novakova, O.; Pizarro, A.M.; Clarkson, G.J.; Liskova, B.; Brabec, V.; Sadler, P.J. Photoactivatable Organometallic Pyridyl Ruthenium(II) Arene Complexes. *Organometallics* **2012**, *31*, 3466–3479, https://doi.org/10.1021/om201177y

7. Battistin, F.; Balducci, G.; Wei, J.; Renfrew, A.K.; Alessio, E. Photolabile Ru Model Complexes with Chelating Diimine Ligands for Light-Triggered Drug Release. *Eur. J. Inorg. Chem.* **2018**, *2018*, 1469–1480, https://doi.org/10.1002/ejic.201701392

8. Liu, Z.; Romero-Canelón, I.; Habtemariam, A.; Clarkson, G.J.; Sadler, P.J. Potent Half-Sandwich Iridium(III) Anticancer Complexes Containing C∧N-Chelated and Pyridine Ligands. *Organometallics* 2014, *33*, 5324–5333. https://doi.org/10.1021/om500644f

9. Martinez, A.; Carreon, T.; Iniguez, E.; Anzellotti, A.; Sanchez, A.; Tyan, M.; Sattler, A.; Herrera, L.; Maldonado, R.A.; Sanchez-Delgado, R.A. Searching for New Chemotherapies for Tropical Diseases: Ruthenium– Clotrimazole Complexes Display High in Vitro Activity against Leishmania major and Trypanosoma cruzi and Low Toxicity toward Normal Mammalian Cells. *J. Med. Chem.* **2012**, *55*, 3867–3877. https://doi.org/10.1021/jm300070h

10. Liu, Z.; Romero-Canelón, I.; Qamar, B.; Hearn, J.M.; Habtemariam, A.; Barry, N.P.E.; Pizarro, A.M.; Clarkson, G.J.; Sadler, P.J. The Potent Oxidant Anticancer Activity of Organoiridium Catalysts. *Angew. Chem., Int. Ed.* **2014**, *53*, 3941–3946. https://doi.org/10.1002/anie.201311161

11. Hackl, C.M.; Legina, M.S.; Pichler, V.; Schmidlehner, M.; Roller, A.; Dömötör, O.; Enyedy, É.A.; Jakupec, M.A.; Kandioller, W.; Keppler, B.K. Thiomaltol-Based Organometallic Complexes with 1-Methylimidazole as Leaving Group: Synthesis, Stability, and Biological Behavior. *Chem. Eur. J.* **2016**, *22*, 17269–17281. https://doi.org/10.1002/chem.201603206

12. Schuecker, R.; John, R.O.; Jakupec, M.A.; Arion, V.B.; Keppler, B.K. Water-Soluble Mixed-Ligand Ruthenium(II) and Osmium(II) Arene Complexes with High Antiproliferative Activity. *Organometallics* **2008**, *27*, 6587–6595. https://doi.org/10.1021/om800774t

13. Enyedy, É.A.; Mészáros, J.P.; Dömötör, O.; Hackl, C.M.; Roller, A.; Keppler, B.K.; Kandioller, W. Comparative solution equilibrium studies on pentamethylcyclopentadienyl rhodium complexes of 2,2′-bipyridine and ethylenediamine and their interaction with human serum albumin. *J. Inorg. Biochem.* **2015**, *152*, 93–103. https://doi.org/10.1016/j.jinorgbio.2015.08.025

14. Dömötör, O.; Pape, V.F.S.; May, N.V.; Szakács, G.; Enyedy, É.A. Comparative solution equilibrium studies of antitumor ruthenium(η^6-*p*-cymene) and rhodium (η^5-C_5Me_5) complexes of 8-hydroxyquinolines. *Dalton Trans.* **2017**, *46*, 4382–4392. https://doi.org/10.1039/C7DT00439G

15. Mészáros, J.P.; Pape, V.F.S.; Szakács, G.; Németi, G.; Dénes, M.; Holczbauer, T.; May, N.V.; Enyedy, É.A. Half-sandwich organometallic Ru and Rh complexes of (N,N) donor compounds: Effect of ligand methylation on solution speciation and anticancer activity. *Dalton Trans.* **2021**, *50*, 8218–8231. https://doi.org/10.1039/D1DT00808K